Int. J. Multiphase Flow Vol. 17, No. 6, pp. 767–782, 1991
Printed in Great Britain.

0301-9322/91 $3.00 + 0.00

FORMATION OF SOLITARY WAVES ON GAS-SHEARED LIQUID LAYERS

C.-A. PENG, L. A. JURMAN and M. J. MCCREADY
Department of Chemical Engineering, University of Notre Dame, Notre Dame, IN 46556, U.S.A.

(Received 2 August 1990; in revised form 5 June 1991)

Abstract—The origin of solitary waves on gas–liquid sheared layers is studied by comparing the behavior of the wave field at sufficiently low liquid Reynolds number, R_L, where solitary waves are observed to form, to measurements at higher R_L where solitary waves do not occur. Observations of the wave field with high-speed video imaging suggest that solitary waves, which appear as a secondary transition of the stratified gas–liquid interface, emanate from existing dominant waves, but that not all dominant waves are transformed. From measurements of interface tracings it is found that for low R_L, waves which have amplitude/substrate depth (a/h) ratios of 0.5–1 occur while for higher R_L, no such waves are observed. A comparison of amplitude/wavelength ratios shows no distinction for different R_L. Consequently, it is conjectured that solitary waves originate from waves with sufficiently large a/h ratios; this change of form being similar to wave breaking. The dimensionless wavenumber is found to be smaller at low R_L, where solitary waves are observed. This suggests that perhaps, larger precursor (to solitary wave) waves are possible because the degree of dispersion, which acts to break waves into separate modes, is lower.

Key Words: gas–liquid flows, interfacial waves, roll waves, atomization, disturbance waves

1. INTRODUCTION

Interfacial waves have been shown to play an important role in determining the pressure drop (Laurinat & Hanratty 1984) and the rate of atomization (Woodmansee & Hanratty 1969; Asali *et al.* 1985; Schadel & Hanratty 1989), which are both important properties of annular gas–liquid flows. Consequently, it is desirable to be able to estimate wave properties to interpret experimental measurements for the design of new equipment. However, general procedures for predicting wave properties for cocurrent annular flows do not exist—primarily owing to the difficulty and complexity of the problem. For example, because of the high degree of gas shear, the liquid flows at conditions which greatly exceed the point of neutral stability of interfacial waves. As a consequence, waves that are present are not small amplitude, periodic waves (as would be expected close to neutral stability) and therefore do not match predictions of wavelength and celerity from linear stability theory. Experiments indicate that these waves may be quite asymmetric, occur irregularly and carry significant liquid—which alters the base state so that the substrate liquid thickness is very different from that which would exist in the absence of waves.

Previous studies of waves in horizontal cocurrent gas–liquid flows by Hanratty & Engen (1957) and Hanratty & Hershman (1961) demonstrated that a transition from periodic waves, to "roll" or "disturbance" waves (which carry significant fluid with them and are not periodic), occurs as the gas flow is increased to produce interfacial shear rates typical of the annular flow regime. Subsequent studies by Miya *et al.* (1971) and Andreussi *et al.* (1985) have defined boundaries of their occurrence and attempted to explain their origin in terms of linear stability theory. Bruno & McCready (1988) provide measurements which suggest that for sufficiently high liquid Reynolds number $R_L = \Gamma/\nu$; where Γ is the liquid volumetric flow per unit width and ν is the kinematic viscosity), roll waves emanate from slowly growing waves which have frequencies much lower than the dominant interfacial waves. For lower R_L, their data suggest that roll waves form by the growth of waves near the peak of the spectrum. For liquids with viscosities in the range of 15 cP, Jurman & McCready (1989) observed that the dominant waves at low R_L (i.e. 5–10) changed from periodic to "solitary" as R_G (the gas Reynolds number) was increased. Jurman *et al.* (1989) speculate that these solitary waves are essentially the same as roll waves except that the interface is continuous and is not breaking or rolling. However, these studies do not resolve the issue of what controls the periodic to solitary transition or determine why solitary waves are observed only at low R_L.

In this paper, the behavior of waves as a function of interfacial shear is examined for liquids of 8–30 cP viscosity at liquid flows low enough for solitary waves to form and also for R_L too large for solitary waves formation. Measurements demonstrate that a transition to solitary waves occurs if the ratio of the wave amplitude to substrate thickness (a/h) of the largest waves approaches unity and that these solitary waves form directly from existing precursor waves. Indirect evidence suggests that this transition does not depend on any qualitative changes in the gas flow, such as separation. If the liquid layer is too thick, no waves with large a/h ratios are observed and this transition never occurs. The pertinent question is thus, why do large a/h waves exist for thin layers but not for larger layers? Some evidence suggests that waves on thinner layers have lower wavenumbers and may be less dispersive. It is spectulated that the degree of dispersion, which acts to break up nonsinuous waves, influences how large the amplitude to substrate depth is likely to be and therefore determines if sufficiently large precursor waves will appear.

2. EXPERIMENTS

(a) Flow system

The experiments presented here were done in a horizontal, rectangular flow channel 30 cm wide, 2.54 cm high and 9 m long. [The flow system is described more completely by Bruno & McCready (1988), Bruno (1988) and Jurman (1990)]. Glycerin–water solutions with viscosities ranging from 8 to 30 cP were used as the liquid. The high aspect ratio rectangular geometry eliminates secondary flow patterns and minimizes side wall effects on the wave field, thus providing (in so far as possible) uniform film and wave properties.

(b) Wave measurements

Instantaneous film height is measured using parallel-wire conductance probes. Their construction is discussed in detail by Miya *et al.* (1971), McCready (1986) and Bruno (1988). Each probe consists of two parallel 0.13 mm dia wires spaced 2 mm apart which extend vertically through the channel, perpendicular to the direction of flow. An input a.c. voltage is supplied to one of the two wires in the form of a 30 kHz sine wave with a voltage of about 0.2 V. The signal is conducted through the liquid to the second wire, where a custom design amplifier/converter circuit measures the conducting current (which is directly proportional to liquid layer thickness) and transforms it into a continuous analog output which is suitable for sampling by a microcomputer. A complete diagram of this circuit, which worked significantly better than previous designs, is given by Jurman (1990). An analog-to-digital conversion rate of 200 samples/s was used. This is appropriate for the conditions studied here where no significant wave frequencies $\gtrsim 50$ Hz were observed. Power spectra of the signals were obtained from samples of $\sim 32{,}000$ data points using FFT techniques described by Bendat & Piersol (1971).

Wave speeds were measured using two parallel-wire conductance probes (Telles & Dukler 1970), displaced by a small distance in the flow direction. The frequency resolution of such probes is determined by the separation distance. Larger separation distances are required to detect and track the longest disturbances, while the highest frequency is effectively determined by a wave whose length equals the separation distance. Therefore, a larger separation distance, z, for the probe increases its ability to resolve the lower frequency modes, but decreases its upper frequency limit. The probes used in this study allow resolution of wave speeds in the approximate range of 3–30 Hz for $z = 1.55$ cm, and 5–50 Hz for $z = 0.55$ cm. Speeds for individual waves can be determined from examining the time delay between the two tracings. Average wave speeds for different modes are obtained by cross-spectral analysis.

(c) Video imaging

The wavefield was viewed using an Ekta-Pro 1000 motion analysis system. The camera was operated at up to 500 frame/s and the resulting tapes viewed at 30 frame/s or sometimes by manually advancing the frames. This arrangement provided clear images of the evolving flow field with enough resolution to discern individual events.

3. EXPERIMENTAL RESULTS

(a) Video imaging

It is of interest first to describe, as well as possible, results that were obtained from viewing the wave field with a high-speed video imaging camera. Presentation of individual frames here is not deemed worthwhile because it would take too many pictures to depict any one event. The wave field was viewed at steady-state conditions and also when the gas flow was increased from zero sufficiently to form solitary waves. Pictures of steady flows revealed that solitary waves often travel for long distances (several feet) catching up to smaller periodic waves and leaving a smooth film behind them on which periodic waves reform [figure 10 in Jurman *et al.* (1989) suggests this]. Solitary waves were observed to form only infrequently, but when they did, they appeared to come from an existing wave. One additional observation from video imaging was that solitary waves which do not span the entire channel width, often would pass other waves which do not span the entire channel and "stick" together at the edges of their fronts to form a wave front which spanned a greater fraction of the channel width. This observation is important because it explains how solitary waves which span most of the channel distance can exist [see figure 10 in Jurman *et al.* (1989)] when none of the precursor 3D waves from which solitary waves could form, have continuous fronts much wider than $\sim 1/3$ of the channel.

When the gas flow was quickly increased ($\sim 1/2$ s for zero to full flow), the entire formation process of a solitary wave could be observed. First, periodic waves with a wavelength of about 2 cm formed, their amplitudes increased and then a fraction of those in the field of view formed into solitary waves. From these video tapes, it is concluded that solitary waves form by continued growth of existing periodic waves—which themselves form as the result of a linear instability of the base film (which may actually be much thinner than the "average" layer thickness). However, not all periodic waves grow into solitary waves. It is further surmised that it is the largest waves which are the ones that form solitary waves. Other experiments, which were done to gain further evidence to support these hypotheses, are presented next.

(b) Wave regime maps

Figure 1 shows maps which were constructed using visual observations of the dominant wave type for 8, 15 and 30 cP liquids. Our primary interest here is solitary waves, which are observed to exist for the low R_L region of each of the three plots at sufficiently high R_G. It is worthwhile to point out several important features which will be discussed further below. First, it is clear that R_L and R_G are not sufficient to completely parameterize the system because the wave map boundaries move with changes in viscosity. Second, the transition from 3D to solitary waves occurs at lower R_G for higher viscosity liquids. Third, solitary waves are confined to low R_L. A final point about the wave maps is that over the range studied, there is no qualitative change in any of the transitions with viscosity.

(c) Surface tracings and wave spectra

The maps of figure 1 suggest that it is appropriate to examine wave behavior as a function of R_G for R_L low enough to allow formation of solitary waves, and R_L too large for this to occur. This procedure will enable comparison of wave behavior leading to the formation of solitary waves with conditions where solitary waves do not form. Figure 2 shows interface tracings for $\mu = 15$ cP and $R_L - 10$ as a function of R_G. At the lowest R_G, waves are sinuous, do not vary much in the transverse direction, but are irregular in amplitude and frequency. The next plot shows a much more uneven surface with a wider range of frequencies present. These data are for 3D waves, so it is noted that a great deal of the irregularity results from a 1D measurement of a wave field which varies in the transverse direction. As a consequence, the probe measures waves with fronts which are not perpendicular to the flow. The fourth tracing is just below the visible transition to solitary waves; it suggests that there may actually be a few solitary waves present (e.g. at $t = 1.2$ s). When viewed in a surface tracing, a solitary wave is asymmetric with a front side that is steeper than the backside and, in addition, the backside is clearly concave-upward. At $R_G = 16, 400$, solitary waves are observed at $t = 0.15, 0.4, 0.6, 0.7, 1.0, 1.25$ and 1.5 s. The rate of solitary waves occurrence continues to increase with R_G with solitary waves occurring with rather irregular time intervals at

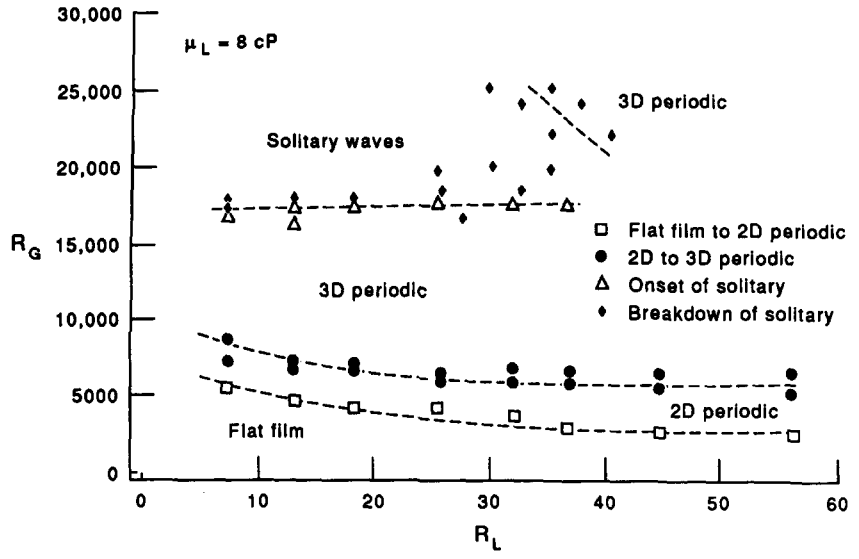

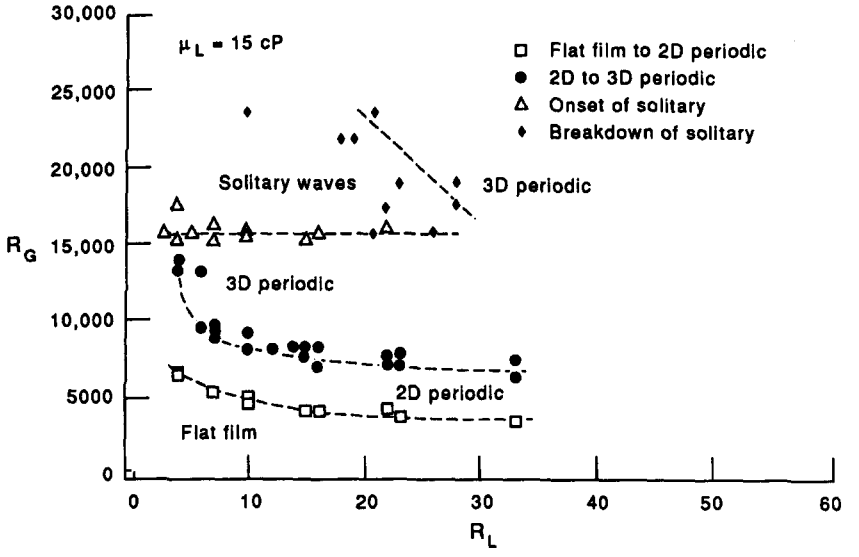

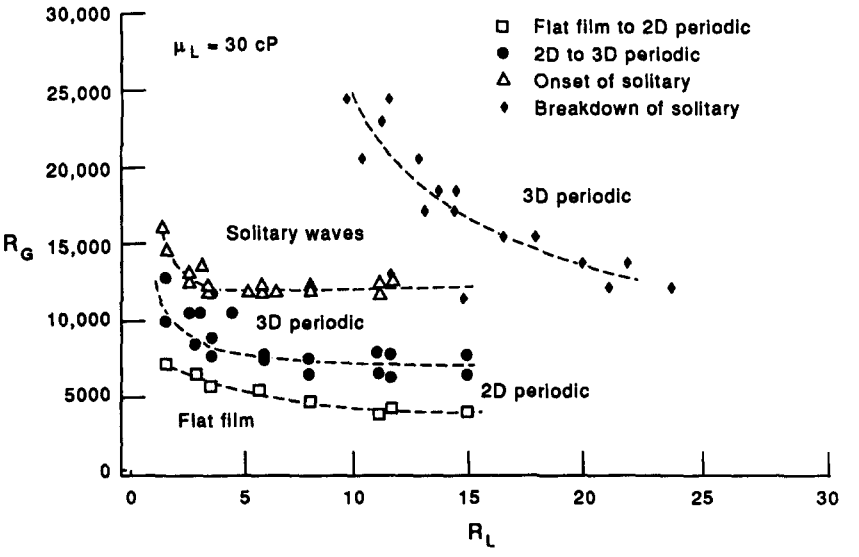

Figure 1. Wave regime maps.

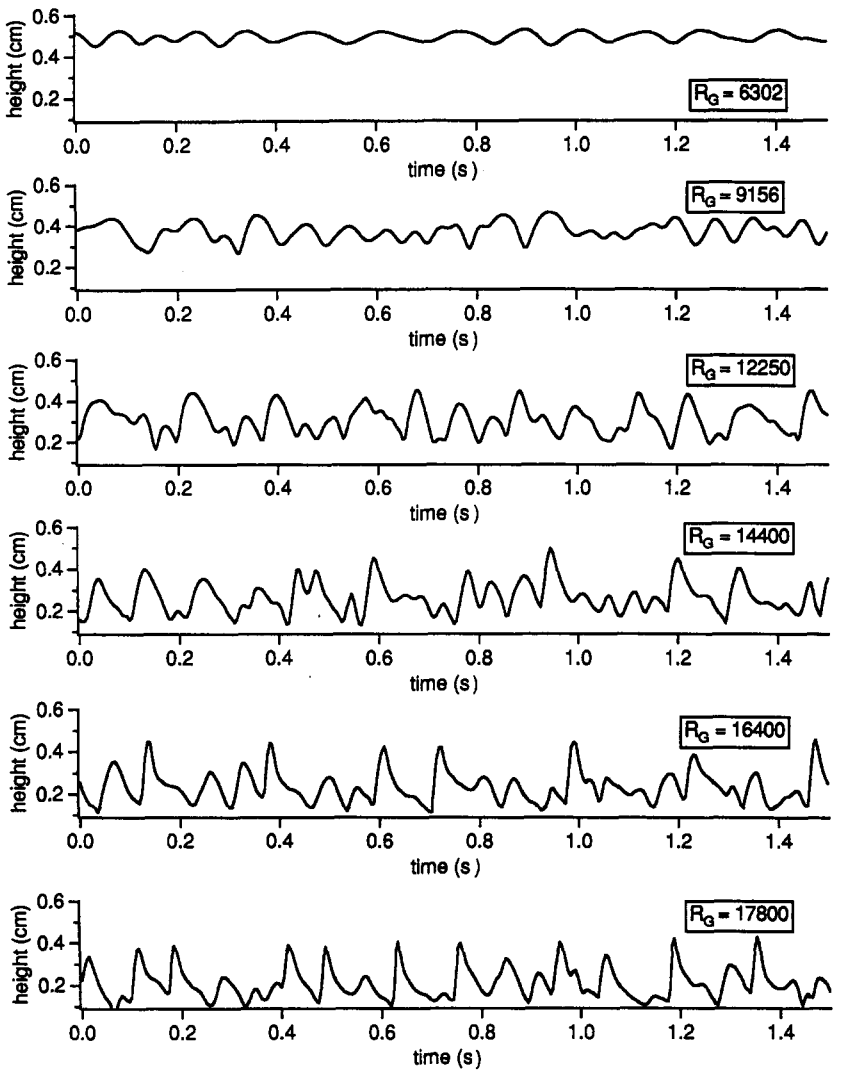

Figure 2. Surface tracings as a function of R_G for $R_L = 10$ and $\mu = 15$ cP.

approx. 5–10/s. It is also interesting to note that a large decrease in the layer depth occurs with the average thickness decreasing from 0.5 to ~ 0.2 cm; the substrate thickness is even lower.

The corresponding power spectra are shown in figure 3. As R_G increases, the amplitude increases and then reaches a limiting value at about $R_G = 14{,}400$, after which it decreases slightly. It is noted that this decrease is due to a reduction of the average liquid thickness because the ratio of average wave amplitude to average liquid thickness continues to increase with R_G. It is clear that the wave spectra do not reflect the regime transitions very well. There is no qualitative change for the 2D to 3D periodic wave transition. The peak at 5 Hz for $R_G = 16{,}400$, is probably associated with the occurrence of solitary waves because they appear in the tracings at about 5/s. However, $R_G = 17{,}820$ shows no distinct peak even though solitary waves are occurring more frequently. It is not surprising that spectral analysis is not particularly informative because a large number of Fourier modes are needed to make the shape of a solitary wave. In addition, solitary waves do not occur periodically.

Experiments corresponding to figures 2 and 3 for $R_L = 47$ are shown in figures 4 and 5. The tracings in figure 4 again increase in irregularity and amplitude with increasing R_G. However, the characteristic solitary wave shapes do not appear. The wave spectra in figure 5 increase in magnitude with increasing R_G and then saturate with little change evident in the last three R_G. As for $R_L = 10$, the decrease in layer depth counteracts the increase in interfacial shear. The spectra

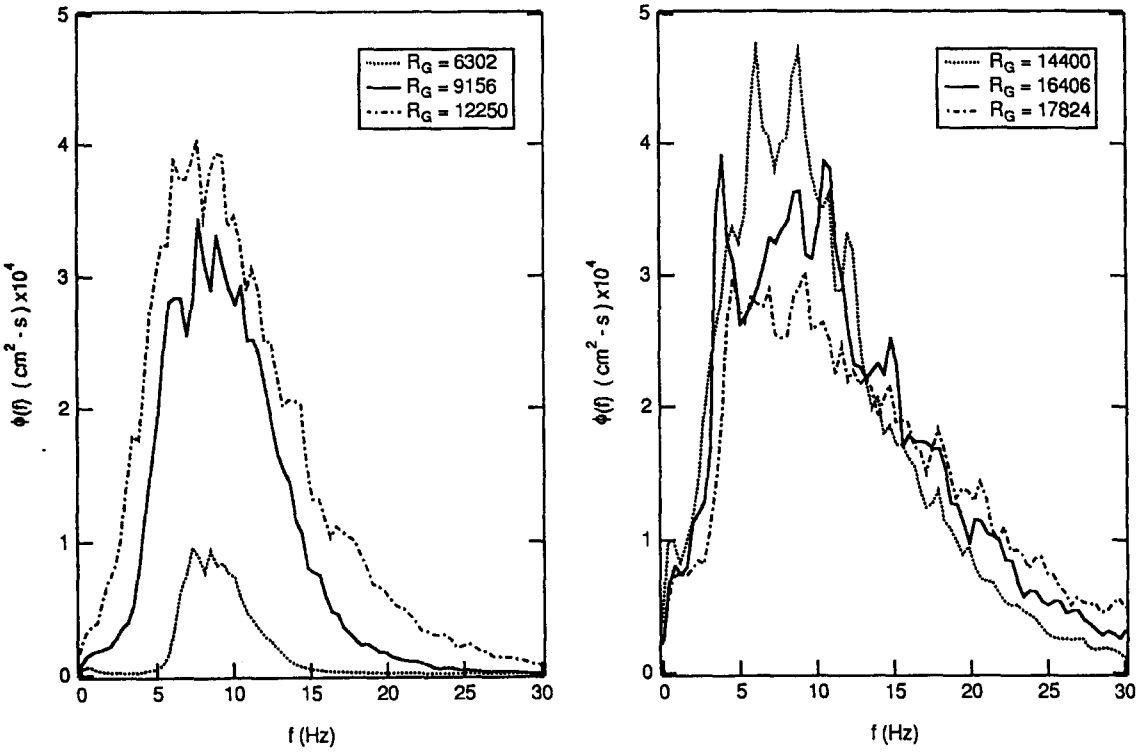

Figure 3. Interfacial wave spectra; $R_L = 10$ and $\mu = 15$ cP.

show the emergence of a distinct low frequency peak which is not present in figure 3. (It is possible to detect the presence of this low frequency oscillation in the baseline of the tracings.) Bruno & McCready (1988) observed such a peak for conditions which were not quite severe enough for roll waves to form. One further point of comparison between the two different R_L is of interest. The wave amplitudes, which are proportional to the square root of the area under the spectral curves, are actually somewhat smaller for $R_L = 47$ (than $R_L = 10$) at higher R_G even though the film thickness is higher.

(d) Wave amplitudes

The data of figures 2–5 do not directly show how, or from what, solitary waves form. Because of the conjecture that solitary waves form from the largest existing waves, the wave tracings were examined to idenfity the largest amplitude waves. This was done by first finding the peaks and then looking for the level of the minima before and after the wave. It was found that, typically, the amplitudes of the largest waves were comparable for both higher and lower R_L. However, to compare the different R_L conditions, it is necessary to nondimensionalize the amplitudes. The amplitudes were first nondimensionalized with their wavelengths. To determine the wavelength, it is necessary to determine the time delay of a given wave between the two probes, and also observe the period of the wave. Because we were not able to develop a reliable automated procedure (i.e. computer algorithm) for doing both of these tasks, the wavelengths were obtained by visually examining the data sets and counting points between the peaks. As this was very time consuming, only the 6 or 7 largest waves at any condition were chosen. Data for the amplitude/wavelength (a/λ) ratios for the largest individual waves for a 15 cP liquid are shown in figure 6. It is seen that for both values of R_L, the largest waves have a/λ ratios in the range 0.1–0.15 but that there is no difference for the two cases. It is next of interest to determine the ratio of amplitude to substrate thickness. The local substrate thickness, h, was obtained from averaging several data points in front of and behind a selected wave. This information could be obtained from the tracing of a single probe and it was possible to reliably code a procedure for finding the waves, and then determining the substrate thickness by averaging several points on both sides of the peak. The a/h ratios, plotted as $2a/h$ vs R_G for three different liquid viscosities in figure 7 using the 10% largest waves (with

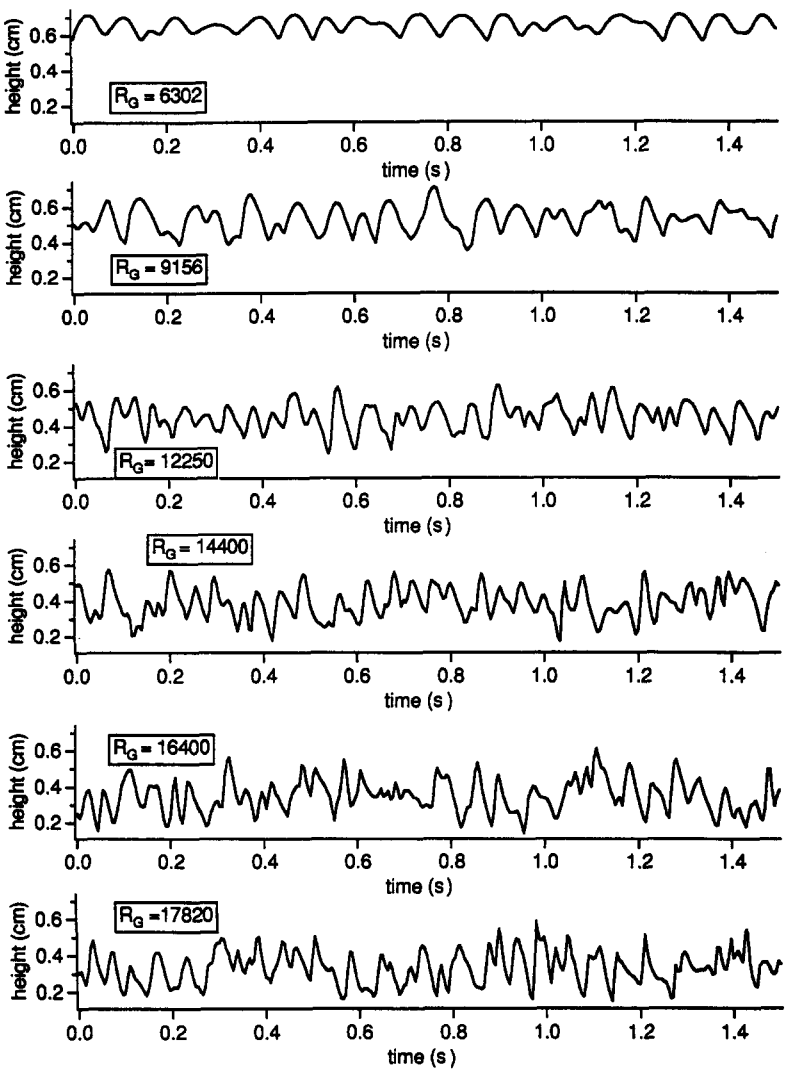

Figure 4. Surface tracings as a function of R_G for $R_L = 47$ and $\mu = 15$ cP.

the error bars representing the standard deviation), show significant results. It is clear that the biggest waves for R_L in the range where solitary waves form, have amplitudes significantly larger than those for higher R_L where solitary waves are not observed. This suggests that solitary waves may be similar to breaking waves (Kinsman 1965) in that the crest moves too fast for the entire disturbance to keep up owing to the retarding effect of the bottom wall. If solitary waves form only from precursor waves with sufficiently large a/h ratios, the issue of solitary waves formation then becomes one of understanding what conditions promote waves with large a/h ratios. It is clear as the layer becomes thicker, the amplitude must get larger to reach the same a/h. Because wave amplitudes generally increase with liquid depth, the pertinent question becomes: what other factors control the maximum wave amplitude and are preventing the amplitude from reaching a sufficiently large value?

(e) Other results

Jurman *et al.* (1989) show plots (for $R_L \cong 5$ to 10) demonstrating that dominant waves travel at velocities close the the predictions of linear stability theory, which predicts a slight decrease in wave celerity as R_G is increased. However, they did not separately measure speeds for the largest amplitude waves which are shown here to have important implications for the formation of solitary waves. Figure 8 shows plots of the average wave speed of the largest 6 or 7 waves, the average

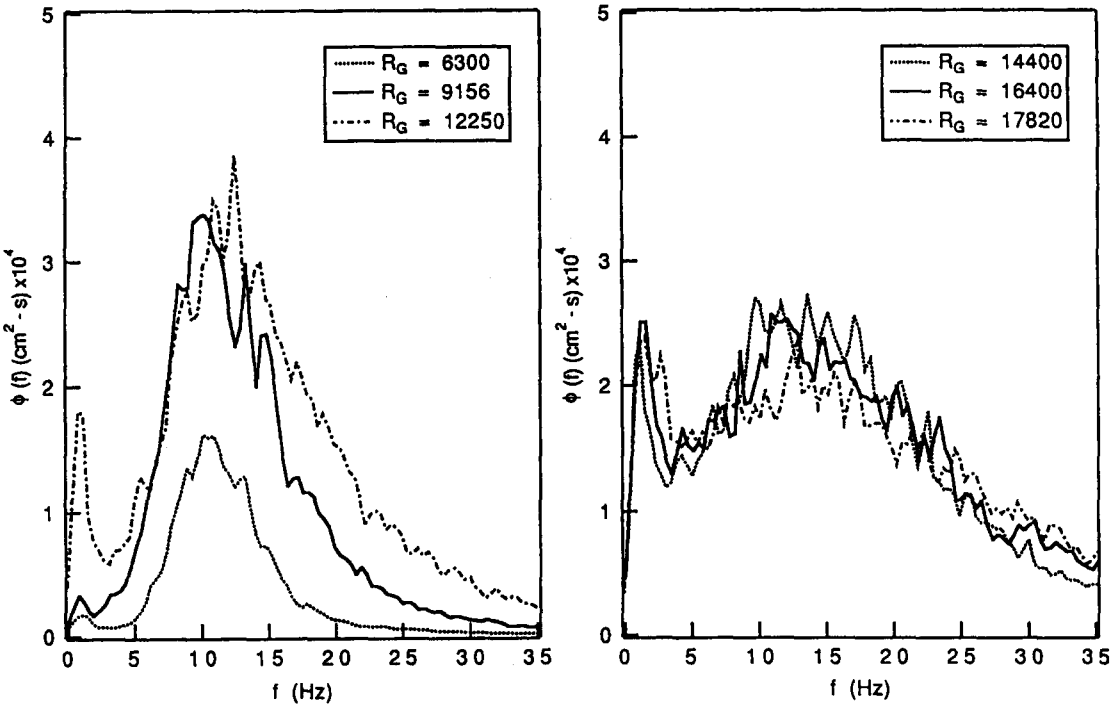

Figure 5. Interfacial wave spectra; $R_L = 47$.

speed of the dominant waves from the peak in the wave spectrum and the interfacial wave velocity. The primary observation to make from figure 8 is that larger amplitude waves travel faster than the average for both values of R_L. Consequently, the evolution of a precursor wave into a solitary wave is not accompanied by a dramatic increase in speed.

It could be suspected that the transition to solitary waves is related to changes in the gas flow. For example, perhaps gas flow separation causes solitary waves to form. Figure 9 shows the properties of some of the largest individual waves plotted as $2\,a/\lambda$ vs α^+, the wavenumber, α, made dimensionless with gas phase turbulence parameters (friction velocity and kinematic viscosity), along with the curve from Zilker & Hanratty (1979) which shows the separated and nonseparated regions for flow over a solid wavy surface. While the waves studied here are not solid, regular and

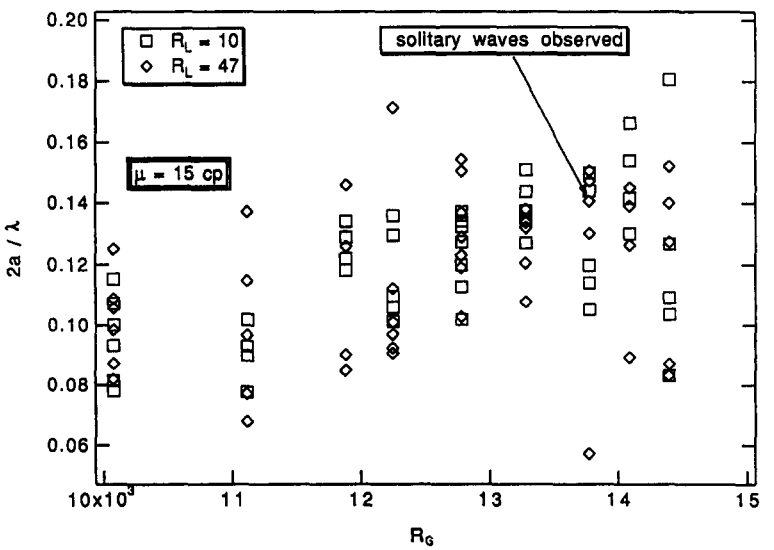

Figure 6. a/λ Ratios for the largest waves.

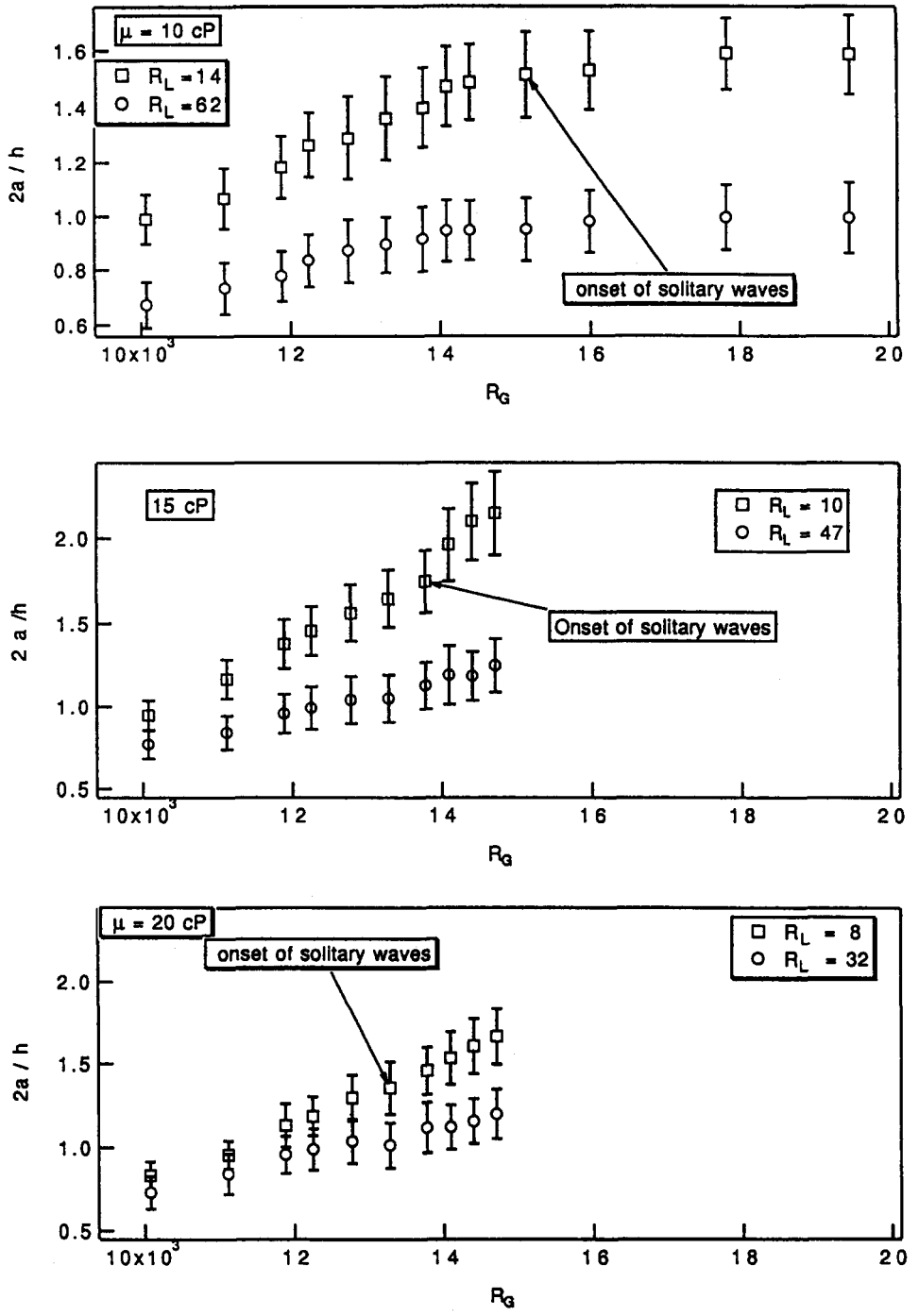

Figure 7. Plots of a/h ratios.

stationary, the gas–liquid viscosity and density ratios are 0.001 and 0.0012, suggesting that the liquid responds on a much slower time scale than the gas and could therefore approximate a solid. Figure 9 indicates that because separation occurs for both low and high R_L, it is not the direct cause of solitary waves formation.

4. DISCUSSION

The data shown above demonstrate that solitary waves form from existing precursor waves which have sufficiently large a/h ratios. However, the obvious question arises, what controls the

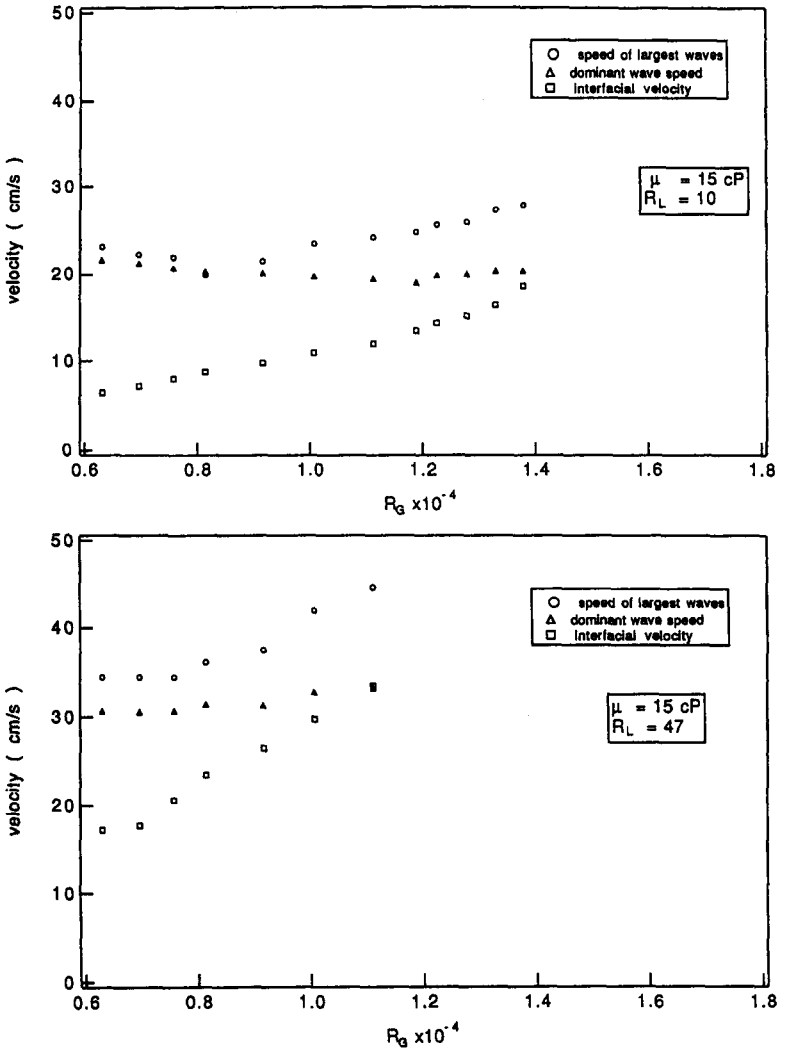

Figure 8. Comparison of interfacial and wave speeds.

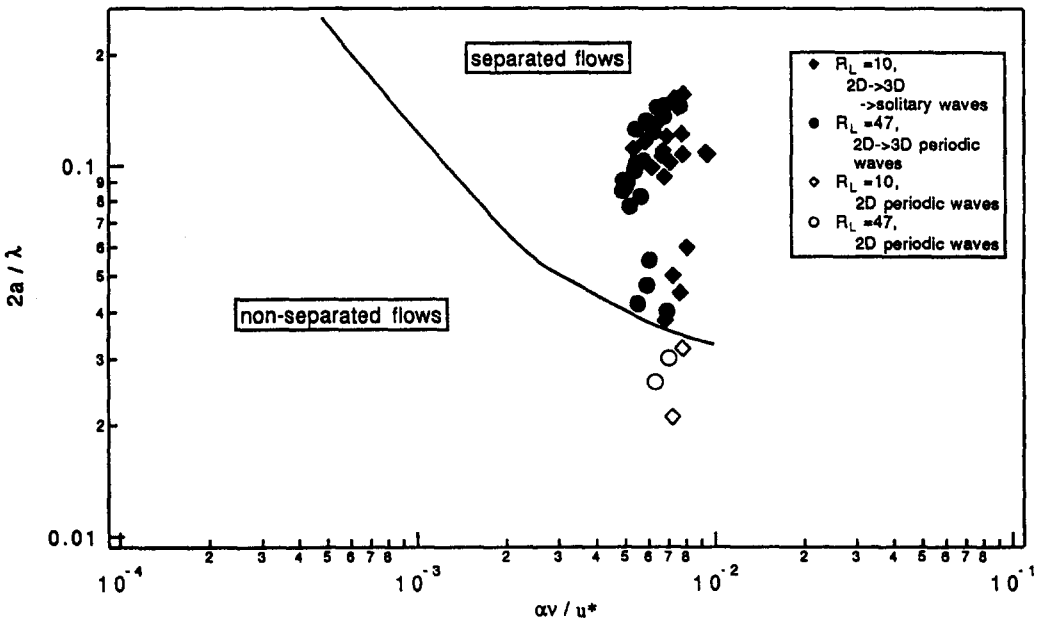

Figure 9. Properties of the largest waves compared with separated and nonseparated flows for flow over solid wavy surfaces.

a/h ratio? To answer this, it is first observed that the largest amplitude waves, other than solitary waves, for either low or high R_L, occur intermittently and are not sinuous in shape. Because they are comprised of a number of modes, an important issue is the degree of dispersion (variation in mode speed with wavenumber), which acts to break up a nonsinuous mode into separate components. An estimate of how the wave speed varies for different modes can be obtained from a wave equation for liquid layers sheared by a gas flow derived by Jurman & McCready (1989) using boundary-layer theory. In the limit of $\alpha R_L = O(1)$, they show that an equation of the form

$$u_t + uu_x + \zeta u^2 + \xi uu_{xx} + \sigma uu_{xxx} + c_0 u_x + pu_{xx} + qu_{xxx} + ru_{xxxx} = 0, \quad [1]$$

where u is the surface position, t is time, x is the flow direction, c_0 is the velocity of a wave with infinite wavelength and p, q and r are the coefficients characterizing forcing, dispersion and dissipation, respectively, is appropriate. The coefficients ζ, ξ and σ are typically small compared with unity and, consequently, the nonlinear terms associated with them will not be considered here. Note that the nonlinear coefficient for the uu_x term can be absorbed into the variable u. Similar simple evolution equations have been shown to approximate the behavior of inviscid water waves on shallow water (Korteweg & deVries 1895), waves on a falling film of moderate R_L (Alekseenko *et al.* 1985) and waves on falling films at very low R_L (Chang 1986). The dispersion relation is readily obtained for a travelling sinuous mode with frequency ω, and infinitesimal amplitude, $u \sim \exp(-i\omega t + i\alpha x)$, as

$$\omega = c_0\alpha - q\alpha^3 + i(p\alpha^2 - r\alpha^4). \quad [2]$$

The real part of ω gives the wave speed is

$$c = c_0 - q\alpha^2. \quad [3]$$

From the imaginary part of ω, the temporal growth rate is

$$\omega_i = p\alpha^2 - r\alpha^4, \quad [4]$$

with wave growth expected if $\omega_i > 0$. Because q is usually < 0, the wave speed increases with α as does the degree of dispersion between different wavenumbers. It is noted that [1] is probably not valid for the higher R_L studied here, however a dispersion relation for sheared layers at high R_L derived by Cohen & Hanratty (1965) (their [39]), gives the same qualitative behavior as [3].

The influence that degree of dispersion might have on the formation of large amplitude precursor waves can be demonstrated by solving [1] for an initial pulse. It is expected, as happens with other similar equations (Lighthill 1978), that dispersion will act to break up any nonsinuous pulse and the nonlinear term will act to keep the pulse together. A simplified version of [1], where ζ, ξ and σ are zero and the term $c_0 u_x$ is transformed away with a moving coordinate, will be used. The physical picture on which the calculations are based is that large amplitude waves exist independent of all other waves so that it is appropriate to solve [1] on an infinite domain. It is suggested that while the wave field below the solitary wave transition consists of "periodic" waves, the largest ones are independent because they occur irregularly and (from figure 8) travel faster than typical waves. A numerical solution can be obtained by using the "hopscotch" method, which is described by Greig & Morris (1976). Details of the implementation are given by Peng (1990). Our present interest is simply to demonstrate the effect of dispersion, so p and r are chosen as small values to make the initial disturbance essentially neutrally stable (actually slightly growing). Figure 10 shows the evolution of the top half of a sine wave pulse, chosen because of its similarity to waves in the data, over 10 time units for two values of q. The increasing asymmetry is caused by the uu_x term which increases the wave slope on the upstream side and decreases it on the other. For $q = 5.0E-5$, the pulse is deformed, but remains as a single wave, however for $q = 1.0E-3$, the higher dispersion has caused the pulse to separate into several modes with lower α to the left and higher α on the right; most of the energy is now in a pulse with a wavelength about 2 twice that of the original. Under normal flow conditions, a mode with wavelength twice that of the peak waves is quickly dissipated (by both direct viscous dissipation and by energy transfer to higher frequency modes) and would not exist. Therefore, the pertinent result of figure 10 is that a pulse breaks up much faster if dispersion is higher. This suggests that as dispersion increases, large amplitude waves are

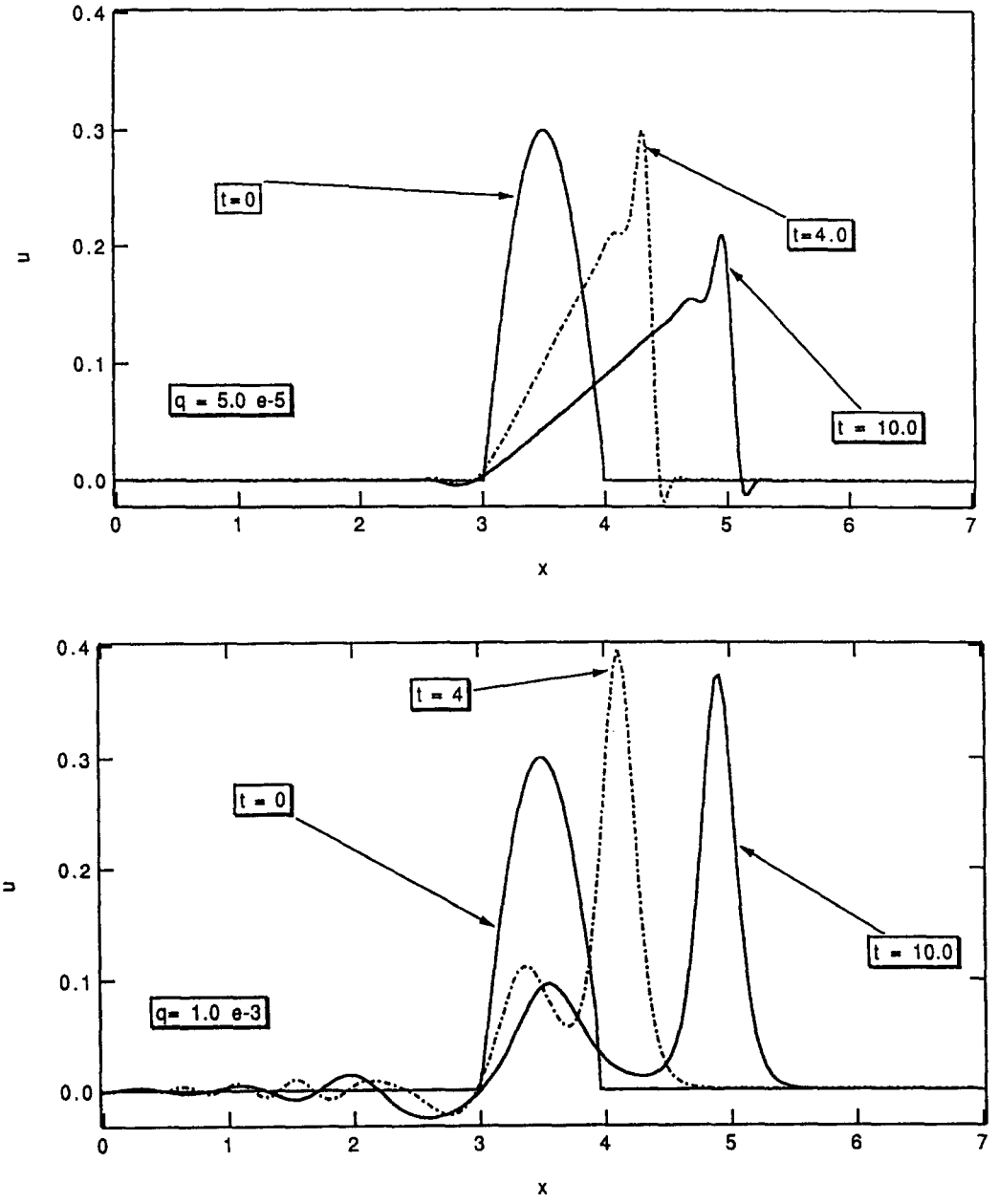

Figure 10. Evolution of a wave pulse with time for low and high dispersion.

less likely to exist without breaking up. It should also be noted that if the parameters are kept the same, and the wavelength increased, a similar degree of breakup will take a longer time.

The solutions shown in figure 10 should be considered primarily as a descriptive model; wave behavior in a real flow is much more complicated. There could be a nonlinear dispersion effect, transverse variation could be important or the time variation could require more than first derivatives. Nevertheless, differences in the degree of dispersion for low and high R_L is a possible explanation for why large precursor waves exist at low R_L and not at higher R_L. At lower R_L the smaller degree of dispersion may allow waves to grow to a larger amplitude without breaking up.

Consequently, it is of interest to examine the data for evidence that thicker layers have either a higher degree of dispersion, or that α is smaller for thinner layers. Figure 11 shows a plot of α for the peak in the wave spectra vs R_G for 15 and 20 cP liquids. For the 20 cP liquid, α values for $R_L = 10$ are well below those for $R_L = 32$ close the solitary wave transition. For the 15 cP fluid, the difference is smaller but still may be significant. (It is noted that if only the largest amplitude

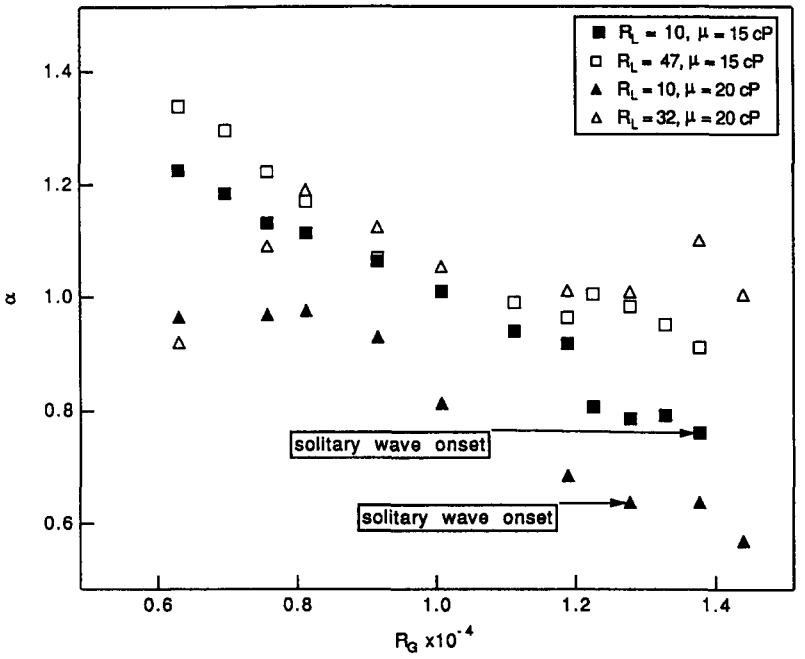

Figure 11. Dimensionless wavenumber as a function of R_G. Solitary waves form from the low α values.

waves are used, similar behavior is observed.) Lighthill (1978) demonstrates that the parameter $a\lambda^2/h^3$ is a measure of the relative importance of nonlinearity to dispersion on a wave. Together, the data of figures 7 and 11 provide values of this parameter, which are shown in table 1, for conditions of solitary wave onset. The values are much larger for the two lower R_L, suggesting that waves at lower R_L are less likely to break up and may grow to larger a/h ratios. One final test of the conjectures regarding dispersion is to compare the slope of the speed vs frequency plots for the region near the peak of the spectrum. A higher slope corresponds to higher dispersion. The values for the slope near the peak are given in table 2. These values are consistent with the notion that dispersion is less for thinner layers, but they do not provide conclusive proof.

From data presented here and previous observations by Hanratty & Hershman (1961), Miya *et al.* (1971), Andreussi *et al.* (1985) and Bruno & McCready (1988), a consistent picture for the formation of both solitary waves and roll waves emerges. If a wave grows to a sufficiently large a/h ratio, further application of force (i.e. shear) causes the wave to become asymmetric with a steeper front and a more shallow back. Depending upon fluid properties, such as viscosity and presumably surface tension, these may either retain a continuous form (solitary waves) or break—producing roll waves. For sufficiently thin layers, waves with wavelengths in the range of dominant waves are able to achieve the amplitude required for this transition. For larger R_L, waves with wavelengths close to the spectral peak cannot attain this a/h ratio, perhaps because of the effect of dispersion. However, at still higher R_L, as evidenced by data of Bruno & McCready (1988) which are replotted as figure 12 (note that similarity to figure 5), a much longer wavelength mode

Table 1. Values for the parameters which control the ratio of nonlinearity to dispersion

μ(cP)	R_L	R_G	$\frac{a\lambda^2}{h^3}$
20	8	12,800	65
20	32	12,800	19
15	10	13,800	52
15	47	13,800	27

Table 2. Comparison of the slope of the wave speed curve at the dominant wave peak for a 20 cP liquid

R_G	f_{peak}, $R_L = 8$	Slope (cm)	f_{peak}, $R_L = 32$	Slope (cm)
6302	7.8	0.863	7.4	3.1
7574	8.5	0.136	9.0	1.1
9156	8.6	1.2	10.2	1.0
10,074	7.7	0.91	10.2	1.2
11,882	7.0	0.7	11.3	1.4
12,777	7.0	0.97	12.5	0.98
13,774	7.4	0.25	14.4	0.58
14,400	7.0	0.291	14.4	0.49

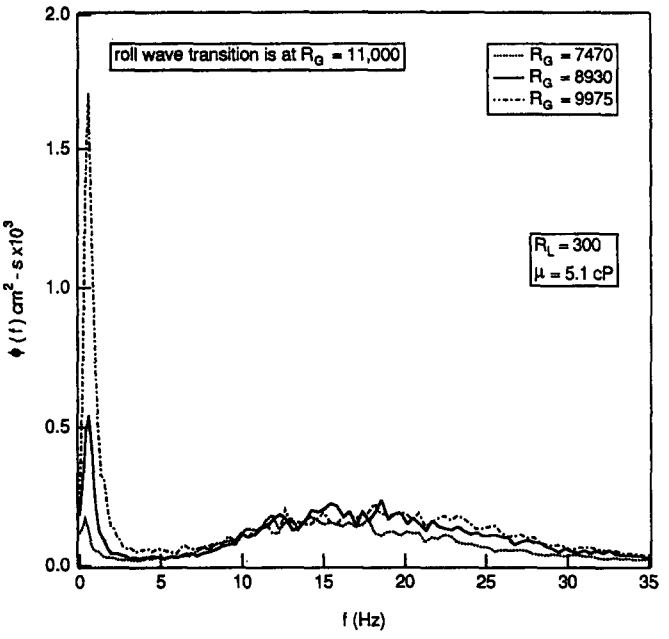

Figure 12. Wave spectra from Bruno & McCready (1988) showing the development below the roll wave transition.

may grow to a sufficient a/h ratio to form roll waves. Note that numerical values for the data of figure 12 are in accord with the data of figure 2. From the magnitude of the spectral data (in figure 12), the average amplitude of the low frequency mode is ~ 0.06 cm, the liquid depth is about 0.65 cm and the wavelength between 15 and 20 cm. Because this mode has a wavelength that is long compared to the film thickness ($\alpha \cong 0.2$), dispersion may again play a minor role. While the average a/h ratio does not yet approach the values in figure 7, the parameter $a\lambda^2/h^3 = 63$, is comparable to the low R_L values of table 1. Furthermore, the largest existing waves are expected to have bigger amplitudes. In addition, for $R_G = 11{,}550$ (not shown in figure 12 because it would be way off scale) the data of Bruno & McCready (1988) show a spectral peak at low frequencies of about 1 order of magnitude higher than for $R_G = 9975$. These waves certainly have amplitudes which are the same order as the substrate thickness.

Finally, it is of interest to discuss the present results in terms of annular pipe flow. For horizontal or nearly horizontal configurations, annular flow can exist over a wide range of conditions which produce different wave structures that will depend upon their location inside the pipe (i.e. top, side, bottom). For situation where the liquid depth on the pipe bottom is sufficiently large, roll waves will be likely to occur and they will contribute to liquid atomization. As the gas velocity is increased, for fixed liquid flow, the fraction of liquid atomized increases with the remaining liquid being distributed more evenly around the pipe. As this happens, the effective film R_L will decrease leading to different wave structures which may range from roll waves on the bottom to "slow waves" (Craik 1966) on the top of the pipe. The association of atomization with large amplitude waves (Woodmansee & Hanratty 1969; Schadel & Hanratty 1989) suggests that the rate of occurrence and amplitude of solitary waves should be the key features of the wave field which control atomization. Eventually, additional increases in the gas flow lead to no further increases in the entrained fraction (Wallis 1969). When this occurs, it is likely that the average liquid thickness and wavelength (which decreases as the liquid thickness decreases) are too small, for a given value of the surface tension, to allow the increase in interfacial curvature associated with formation of solitary waves. A Weber number of the form $\rho u^{*2}\lambda/\gamma$, where u^* is the friction velocity, γ is the coefficient of surface tension and λ is for typical existing waves on the very thin film [a form suggested by Andreussi (1980) for the onset of atomization], may reach a limiting value too small for additional atomization in a fashion similar to what happens at lower R_G before the onset of atomization. At very high R_G, an increase in gas

shear simply decreases the liquid thickness (and therefore wavelength); a further increase in the rate of atomization does not occur.

5. CONCLUSIONS

Solitary waves, which appear as a secondary transition of the stratified gas–liquid interface, emanate from existing precursor waves, that have wavelengths close the the spectral peak and sufficiently large amplitude/film ratios. This transition process occurs by a change of shape that is similar to wave breaking. Such large waves are favored on thinner layers and do not seem to occur on thicker layers where a larger amplitude would be required. The dimensionless wavenumber of the largest amplitude waves on thinner layers appears to be smaller than for thicker layers and the parameter $a\lambda^2/h^3$ is much larger. This suggests that the degree of dispersion, which decreases with decreasing wavenumber and will act to break up nonsinuous waves, may play an important role in determining if potential precursor waves can grow to sufficient amplitude to evolve into solitary waves. At much higher R_L, roll waves form by a similar mechanism except that the precursor waves are modes with wavelengths much longer than waves at the peak of the spectrum.

Acknowledgements—This work is being supported by the Department of Energy under Grant DE-FG02-88ER13913. Additional support for this research equipment from the Chevron Corporation is also acknowledged.

REFERENCES

ALEKSEENKO, S. V., NAKORYAKOV, V. YE. & POKUSAEV, B. G. 1985 Wave formation on a vertical falling film. *AIChE Jl* **31,** 1446–1460.

ANDREUSSI, P. 1980 The onset of entrainment in annular downward flows. *Can. J. chem. Engng* **58,** 267–270.

ANDREUSSI, P., ASALI, J. C. & HANRATTY, T. J. 1985 Initiation of roll waves in gas–liquid flows. *AIChE Jl* **31,** 119–126.

ASALI, J. C., LEMAN, G. W. & HANRATTY, T. J. 1985 Entrainment measurements and their use in design equations. *PhysicoChem. Hydrodynam.* **6,** 207–221.

BENDAT, J. S. & PIERSOL, A. G. 1971 *Random Data: Analysis and Measurement Procedures.* Wiley-Interscience, New York.

BRUNO, K. 1988 The study of interfacial waves in gas–liquid flows. Ph.D. Thesis, Univ. of Notre Dame, Ind.

BRUNO, K. & MCCREADY, M. J. 1988 Origin of roll waves in horizontal gas–liquid flows. *AIChE Jl* **34,** 1431–1440.

CHANG, H.-C. 1986 Nonlinear waves on liquid film surface—I. Flooding in a vertical tube. *Chem. Engng Sci.* **42,** 2463–2475.

COHEN, L. S. & HANRATTY, T. J. 1965 Generation of waves in the cocurrent flow of air on a liquid. *AIChE Jl* **11,** 138–144.

CRAIK, A. D. D. 1966 Wind-generated waves in thin liquid films. *J. Fluid Mech.* **26,** 369.

GREIG, I. S. & MORRIS, J. L. 1976 A hopscotch method for the Korteweg–de Vries equation. *J. comput. Phys.* **20,** 64.

HANRATTY, T. J. & ENGEN, J. M. 1957 Interaction between a turbulent air stream and a moving water surface. *AIChE Jl* **3,** 299–308.

HANRATTY, T. J. & HERSHMAN, A. 1961 Initiation of roll waves. *AIChE Jl* **7,** 488–497.

JURMAN, L. A. 1990 Interfacial waves on sheared, thin liquid films. Ph.D. Thesis, Univ. of Notre Dame, Ind.

JURMAN, L. A. & MCCREADY, M. J. 1989 Study of waves on thin liquid films sheared by turbulent gas flows. *Phys. Fluids* **A1,** 522–536.

JURMAN, L. A., BRUNO, K. & MCCREADY, M. J. 1989 Characterization of waves on thin, horizontal, gas-sheared liquid films. *Int. J. Multiphase Flow* **15,** 371–384.

KINSMAN, B. 1965 *Wind Waves.* Prentice-Hall, Englewood Cliffs, N.J.

KORTEWEG, D. J. & DE VRIES, G. 1895 On the change of form of long waves advancing in a rectangular canal and on a new type of long stationary wave. *Phil. Mag.* **39,** Series 5, 422.

LAURINAT, J. E. & HANRATTY, T. J. 1984 Pressure drop measurements for annular gas–liquid flow. *Int. J. Multiphase Flow* **10,** 341–356.

LIGHTHILL, J. 1978 *Waves in Fluids.* Cambridge Univ. Press, Cambs.

MCCREADY, M. J. 1986 Spectral behavior of capillary waves in gas–liquid flows. *Phys. Fluids* **29,** 2836–2842.

MIYA, M., WOODMANSEE, D. E. & HANRATTY, T. J. 1971 A model for roll waves in gas–liquid flows. *Chem. Engng Sci.* **26,** 1915–1923.

PENG, C.-A. 1990 The formation of solitary waves in horizontal gas–liquid concurrent flows. M. S. Thesis, Univ. of Notre Dame, Ind.

SCHADEL, S. A. & HANRATTY, T. J. 1989 Interpretation of atomization rates of the liquid film in gas–liquid annular flow. *Int. J. Multiphase Flow* **15,** 893–900.

TELLES, A. S. & DUKLER, A. E. 1970 Statistical characteristics of thin, vertical wavy liquid films. *Ind. Engng Chem. Fundam.* **9,** 412–421.

WALLIS, G. B. 1969 *One-dimensional Two-phase Flow*, pp. 390–392. McGraw-Hill, New York.

WOODMANSEE, D. E. & HANRATTY, T. J. 1969 Mechanism for the removal of droplets from a liquid surface by a parallel air flow. *Chem. Engng Sci.* **24,** 299–307.

ZILKER, D. P. & HANRATTY, T. J. 1979 Influence of the amplitude of a solid wavy wall on a turbulent flow. Part 2: separated flows. *J. Fluid Mech.* **90,** 257.